Fine Structure and Dynamics of the Solar Atmosphere
Proceedings IAU Symposium No. 327, 2016
S. Vargas Domínguez, A.G. Kosovichev, P. Antolin & L. Harra, eds.

doi:10.1017/S1743921317001818

Magnetic field line braiding in the solar atmosphere

S. Candelaresi, D. I. Pontin and G. Hornig
Division of Mathematics, University of Dundee, Dundee, DD1 4HN, UK

Abstract. Using a magnetic carpet as model for the near surface solar magnetic field we study its effects on the propagation of energy injectected by photospheric footpoint motions. Such a magnetic carpet structure is topologically highly non-trivial and with its magnetic nulls exhibits qualitatively different behavior than simpler magnetic fields. We show that the presence of magnetic fields connecting back to the photosphere inhibits the propagation of energy into higher layers of the solar atmosphere, like the solar corona. By applying certain types of footpoint motions the magnetic field topology is is greatly reduced through magnetic field reconnection which facilitates the propagation of energy and disturbances from the photosphere.

Keywords. Sun: photosphere – Sun: magnetic fields – Sun: sunspots – magnetic reconnection – magnetohydrodynamics (MHD) – plasmas

1. Introduction

In many studies of the solar magnetic field, it is assumed that the field connects one area of the active region with another thorugh a loop like fields. In such models that loop extends to various heights in the solar atmosphere and is sometimes assumed to be twisted or braided. In any case, the field does not immediately connect back to the same region. However, observations have shown that the field exhibits much more complex structures which includes null points where the magnetic field vanishes (Longcope 2003; Gošić 2014; Platten 2014; Edwards 2015). Their presence severely alters the propagation of energy from the photosphere along the magnetic field. In this work we analyze the effects of such highly non-trivial magnetic field line topology on the energy propagation. For that we impose an artificial driver at the lower boundary of our domain and measure the Poynting flux along the magnetic field lines.

2. Model

As non-trivial test case we use an initial magnetic field that is created by three magnetic monopoles residing outside the computational domain (Candelaresi 2016). They are located at $\boldsymbol{x}_1 = (0, 0, -0.85)$, $\boldsymbol{x}_2 = (2, 0, -0.85)$ and $\boldsymbol{x}_3 = (-2, 0, -0.85)$ and give rise to the magnetic vector potential

$$\boldsymbol{A} = \boldsymbol{A}_0 + B_0 \sum_{i=1}^{n} \epsilon_i \frac{\boldsymbol{e}_z \times (\boldsymbol{x} - \boldsymbol{x}_i)}{|\boldsymbol{x} - \boldsymbol{x}_i|^3}, \tag{2.1}$$

where $\boldsymbol{A}_0$ gives rise to the background magnetic field $\boldsymbol{B}_0 = \boldsymbol{\nabla} \times \boldsymbol{A}_0 = B_0 \hat{\boldsymbol{e}}_z$. Throughout the simulations we will use $B_0 = 0.1$. This initial field condition is shown in Figure 1.

We place the magnetic field inside a box of size $8 \times 8 \times 16$ (xyz) with a grid resolution of $256 \times 256 \times 512$. Flows through the side boundaries (xy) and the lower boundary $(z = 0)$ are set to zero, while the upper boundary is open for the fluid flow. The side boundaries are chosen to be magnetically closed (perfect conductors) while the top is magnetically open. At the lower boundary we impose a potential field extrapolation. In order to simulate a system that is open for magnetic waves, we design the upper half of our computational domain $(z > 8)$ such that

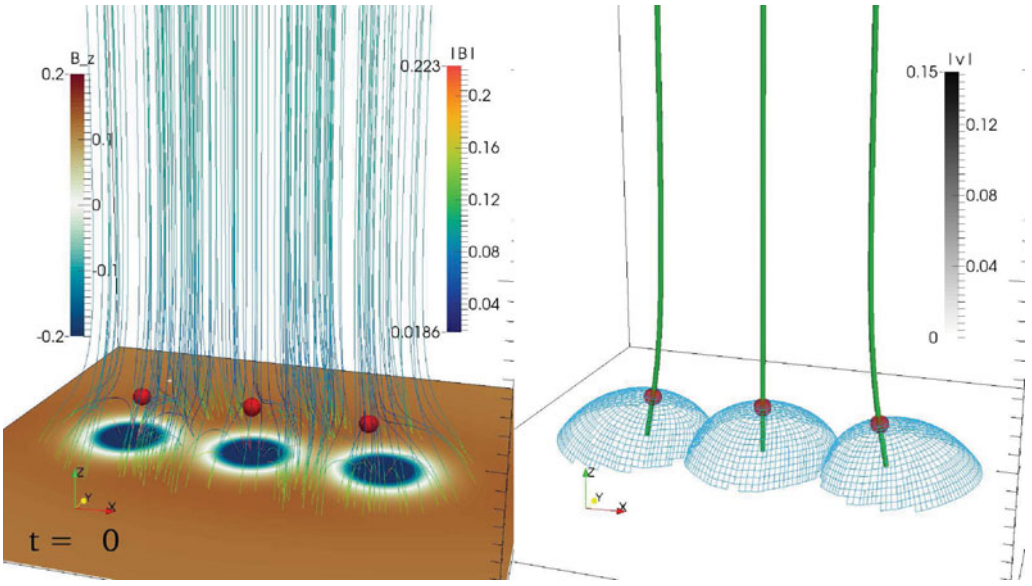

Figure 1. Initial magnetic field with the vertical component on the lower boundary and magnetic null points as red spheres (left). Colours denote the field strength while the gray scale denotes the boundary velocity (not switched on at $t = 0$). The right panel shows the magnetic nulls as red sphere, separatrix layers as blue wire frame and the magnetic spines as green tubes.

any waves are effectively being damped. We achieve this by sharply increasing the viscosity by a factor of 8 as compared to the lower half of the domain.

Since in this work we are mainly interested in the effects of the magnetic field line topology we apply a model for an isothermal atmosphere without density stratification. We also do not take into account temperature effects. For that we solve the magnetohydrodynamics (MHD) equations for a resistive, viscous, compressible and isothermal gas

$$\frac{\partial \boldsymbol{A}}{\partial t} = \boldsymbol{u} \times \boldsymbol{B} + \eta \nabla^2 \boldsymbol{A}, \tag{2.2}$$

$$\frac{\mathrm{D}\boldsymbol{u}}{\mathrm{D}t} = -c_\mathrm{s}^2 \boldsymbol{\nabla} \ln \rho + \boldsymbol{J} \times \boldsymbol{B}/\rho + \boldsymbol{F}_\mathrm{visc}, \tag{2.3}$$

$$\frac{\mathrm{D} \ln \rho}{\mathrm{D}t} = -\boldsymbol{\nabla} \cdot \boldsymbol{u}, \tag{2.4}$$

with the magnetic vector potential $\boldsymbol{A}$, the magnetic field $\boldsymbol{B} = \boldsymbol{\nabla} \times \boldsymbol{A}$, velocity $\boldsymbol{u}$, constant magnetic resistivity η, Lagrangian time derivative $\mathrm{D}/\mathrm{D}t = \partial/\partial t + \boldsymbol{u} \cdot \boldsymbol{\nabla}$, sound speed c_s, density ρ, electric current density $\boldsymbol{J} = \boldsymbol{\nabla} \times \boldsymbol{B}$ and viscous forces $\boldsymbol{F}_\mathrm{visc}$. The viscous forces are given as $\boldsymbol{F}_\mathrm{visc} = \rho^{-1} \boldsymbol{\nabla} \cdot 2\nu\rho\boldsymbol{S}$, with the kinematic viscosity ν, and traceless rate of strain tensor $\boldsymbol{S}_{ij} = \frac{1}{2}(u_{i,j} + u_{j,i}) - \frac{1}{3}\delta_{ij} \boldsymbol{\nabla} \cdot \boldsymbol{u}$. Being an isothermal gas we have $p = c_\mathrm{s}^2 \rho$ for the pressure. For the vector potential $\boldsymbol{A}$ we apply the Weyl gauge with $\boldsymbol{\nabla} \cdot \boldsymbol{A} = 0$. As parameters we choose $\eta = 4 \times 10^{-4}$ and $\nu = 4 \times 10^{-3}$.

For the boundary driver at $z = 0$ we choose a so called blinking vortex motion which consists of two circular motions centered at $(1, 0, 0)$ and $(-1, 0, 0)$ (see Figure 2). Those two circular motions are switched on and of in an alternating way which gives rise to a very efficient mixing of magnetic field polarities at the lower boundary. Since a simple stipulation of velocity would lead to unphysical behavior we apply a driver that is forcing the fluid from it's current velocity $\boldsymbol{u}$ to the desired driver velocity $\boldsymbol{u}_\mathrm{d}$ via an exponential saturation. It's form is given as

$$\frac{\partial \boldsymbol{u}}{\partial t} = (\boldsymbol{u} - \boldsymbol{u}_\mathrm{d})/\lambda_u, \tag{2.5}$$

https://doi.org/10.1017/S1743921317001818 Published online by Cambridge University Press

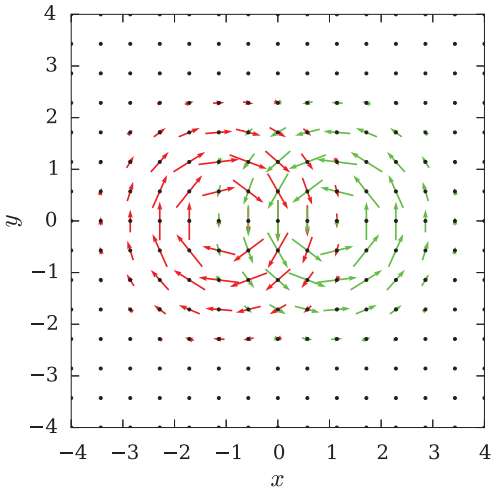

Figure 2. Forced velocity field at the lower boundary at different times in red (left) and green (right). In our simulations we switch between the two driving vortices every 32 code time units.

with the saturation half time $\lambda_u = 0.01$. The driver profile is chosen such that it provides a high level of mixing of magnetic field polarities and is given as

$$\begin{aligned} u_{\rm d}^x(x,y,0) &= \pm u_0 \exp\left[(-(x \mp x_c)^2 - y^2)/2 - \right. \\ &\quad \left. (\mathrm{mod}(t, t_{E3}))^2/(t_{E3}/4)^2\right](-y) \qquad (2.6) \\ u_{\rm d}^y(x,y,0) &= \pm u_0 k_c \exp\left[(-(x \mp x_c)^2 - y^2)/2 - \right. \\ &\quad \left. (\mathrm{mod}(t, t_{E3}))^2/(t_{E3}/4)^2\right](x \mp x_c) \qquad (2.7) \\ u_{\rm d}^z(x,y,0) &= 0, \qquad (2.8) \end{aligned}$$

with the time $t_{E3} = 32$. The plus and minus signs are chosen such that we obtain a so called blinking vortex motion with

$$\pm = \begin{cases} + & \text{if} \quad \mathrm{mod}(\mathrm{int}(t/t_{E3}), 2) = 0 \\ - & \text{if} \quad \mathrm{mod}(\mathrm{int}(t/t_{E3}), 2) \neq 0 \end{cases}, \qquad (2.9)$$

with the integer function int.

3. Results

At early times, with the magnetic field topology intact, we observe that disturbances from the lower boundary, imposed by the velocity driver, do not travel to higher altitudes. This can be clearly seen as we measure the averaged Poynting flux in the vertical direction $\langle(\boldsymbol{E} \times \boldsymbol{B})_z\rangle_{xy}$, where $\boldsymbol{E}$ is the electric field and the averages are taken over horizontal planes (Figure 3).

The reason for this inhibition is of course the presence of closed magnetic field lines which connect back to the photosphere. Such a field gives rise to magnetic null points and separatrix layers. However, as soon as the initial magnetic field topology is broken up and simplified we obtain a field that is better connected to the upper boundary and hence allows for energy fluxes from the lower tot the upper boundary.

Simultaneously, we also observe the disappearance of magnetic nulls through the lower boundary (Figure 4). Their disappearance is aided by the shredding of the magnetic field through the imposed boundary motions.

https://doi.org/10.1017/S1743921317001818 Published online by Cambridge University Press

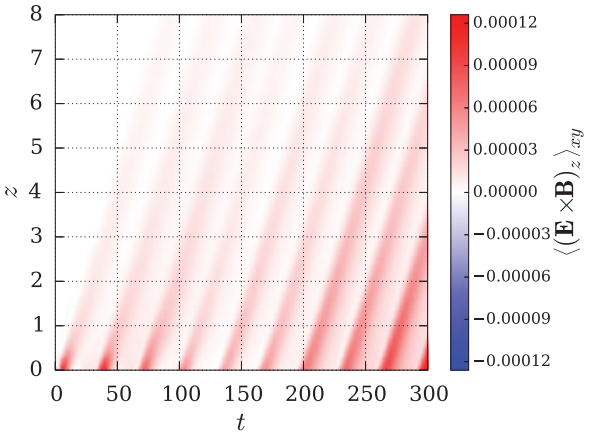

Figure 3. Horizontally averaged vertical Poynting flux in dependence of time t and height z.

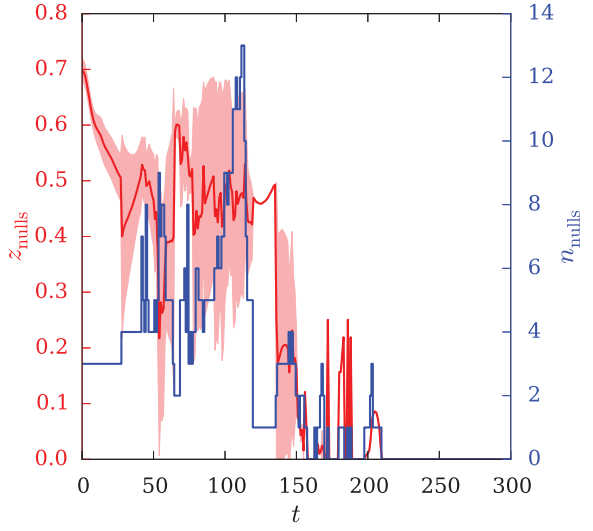

Figure 4. Average height of the magnetic null points (red line) with standard deviation (light red shading) with the number of magnetic nulls (blue line).

4. Conclusions

We have demonstrated that the presence of a magnetic carpet structure with magnetic null points and closed (to the surface) magnetic fields strongly inhibits the propagation of disturbances and energy from the photosphere to higher layers. However, by imposing a driver, that non-trivial magnetic field topology is simplified by shredding of magnetic null points and separatrix surfaces. This leads to an increased energy flux to higher layers.

By using a simplified model with an isothermal atmosphere with constant sound speed we were able to focus on the effects of the field topology. More realistic models need to include effects from temperature, density stratification and a more realistic footpoint driver. The latter can be achieved through photospheric measurements and local correlation tracking which extracts the horizontal velocity field. However, while more realistic modeling of the atmosphere may change the dynamics of the shredding process we don't expect it to affect the main result. A simplification of the topology has to occur, since the Poynting flux of the driver cannot be supported by the carpet field.

https://doi.org/10.1017/S1743921317001818 Published online by Cambridge University Press

Acknowledgements

The author acknowledges financial support from the UK's STFC (grant number ST/K000993).

References

Longcope, D. W., Brown, D. S., & Priest, E. R. 2003, *Phys. Plasmas*, 10, 3321

M. Gošić, L. R. Bellot Rubio, D. Orozco Suárez, Y. Katsukawa, & J. C. del Toro Iniesta 2014, *ApJ*, 797, 49

Platten, S. J., Parnell, C. E., Haynes, A. L., Priest, E. R., & Mackay, D. H. 2014, *A&A*, 565, A44

Edwards, S. J. & Parnell, C. E. 2015, *Sol. Phys*, 290, 2055

Candelaresi, S., Pontin, D. I., & Hornig, G. 2016, *ApJ*, 832, 150